ISSN 2354-9114 (online), ISSN 0024-9521 (print)
Indonesian Journal of Geography Vol 54, No 3 (2022): 333-343
DOI: 10.22146/ijg.60659 website: https://jurnal.ugm.ac.id/ijg

INDONESIAN JOURNAL OF GEOGRAPHY

RESEARCH ARTICLE

Preliminary Study on the Use of Digital Surface Models for Estimating Vegetation Cover Density in a Mountainous Area

Projo Danoedoro[1], Diwyacitta Dirda Gupita[2], Muhammad Zayyanul Afwani[1] Haeydar Anggara Hadi[1], William Krista Mahendra[1]

[1]Remote Sensing Laboratory, Department of Geographical Information Science, Faculty of Geography, Universitas Gadjah Mada, Indonesia

[2]Department of Geography, NTNU (Norwegian University of Science and Technology), NO-7491, Trondheim, Norway

Received: 2020-12-28
Accepted: 2022-10-13

Keywords:
digital surface model; forest cover density; vegetation index; vegetation volume index

Correspondent Email:
projo.danoedoro@geo.ugm.ac.id

Abstract Digital surface model (DSM) has been widely available for mapping and was also sometimes used for mapping vegetation height. The authors conducted a preliminary study to evaluate the potential use of DSMs derived from ASTER, ALOS, and SRTM for estimating vegetation cover density in mountainous area. This study used NDVI and SAVI vegetation indices, in addition to forest cover density (FCD) model as references for evaluation. A DSM-based volume index (Volindex) concept is introduced, which is the product of the canopy height model (CHM) and the pixel area. CHM was derived from the value difference between the DSM and the reference DEM. The Volindex model was then compared with the NDVI, SAVI and FCD. We found that all DSM-based Volindex models are not accurate enough to represent the vegetation cover density, although the ALOS Palsar-based Volindex could reach 41.53% accuracy and was finally used to predict the vegetation cover density.

1. Introduction

Nowadays, the availability of images in the form of digital surface models (DSM) is increasing. This is inseparable from the development of imaging systems that can derive data for this purpose, both those working in the passive optical (producing stereoscopic images), active optical (Lidar), and in the active microwave domains (in this case radar). Among these various systems, DSM recorded via satellite is a type of data that is widely available and has attracted interest for use in various applications, for example ASTER GDEM, SRTM, and ALOS Palsar.

From a geographical point of view the DSM differs from the digital elevation model (DEM), in terms of the elevation information presented (Huggett and Cheesman, 2002). DEM provides ground level information above a datum or an agreed reference, while DSM provides information on the height of land cover such as vegetation and buildings, and the ground level if the land is open without cover. Due to its capability to provide information on the height of land cover, DSM data has been widely studied and applied for various purposes around the world, for example for the measurement of tree height (Kellndorfer *et al*., 2004; Urbazaev *et al*., 2018), urban green (Hecht *et al*., 2008), time-series analysis of vegetation (Trier *et al*., 2018), and also mapping of plant species (Wu *et al*., 2016), in addition to topographic mapping (Julzarika and Harintaka , 2019).

Despite their difference, many researchers have used DSM as DEM, both for topographic mapping (Nikolakopoulos and Chrysoulakis, 2006), physiographic interpretation (Taramelli and Melelli, 2008), flood hazard mapping and other DEM-based modeling (Prasannakumar *et al.,* 2011; Dragut and Elsank, 2011; Dragut *et al*., 2012). Some of these studies ignored the differences between DEM and DSM, and some others considered that the method of recording by the sensor and the use of the selected electromagnetic wavelength spectrum minimizes the difference in elevation between the land surface and the land cover height.

Broadly speaking, field analysis does not require accurate DSM corrections, if it is related to visual interpretations; but it requires accurate corrections to DEM when used as a basis for modeling terrain attributes of slope, flow direction, flow accumulation, and models related to topo shape (Eastman, 2020). Huggett and Cheesman (2002) stated that the accuracy of a DEM is highly dependent on the accuracy of the source data. The accuracy of DEM is never greater than that of the source data. Besides, the accuracy is very dependent on the modeling methods, but on the other hand usually the method of obtaining the error value is not explained in detail. Furthermore, some applications rarely carried out test for the distribution of errors in the model. The method used to produce error values does not evaluate DEM for different types of errors (random and systematic).

On the contrary, research related to vegetation as land cover and its function in the ecosystem is mostly carried out using optical images. Various approaches to extracting vegetation parameter information have been carried out with optical digital images, for example through multispectral classification of various land cover classes or multispectral classification combined with GIS to identify ecosystem units (Danoedoro, 2019), transformation of vegetation indices for study of vegetation density and biomass estimation (Huete 1988; Dewa and Danoedoro, 2017), and also classification of vegetation structural composition through forest cover density

or FCD (Himayah *et al.,* 2016; Ismail *et al.,* 2017; Salsabila and Danoedoro, 2021; Danoedoro and Gupita, 2022). Vegetation studies using vegetation indices in Menoreh Mountain have been carried out by Umarhadi *et al.* (2018) and Umarhadi and Danoedoro (2019).

Based on the introduced background, the research problem could be formulated that DSM has not been studied much for ecological vegetation studies in mountainous wet tropical areas like Indonesia, even though DSM contains information on vegetation height. Research carried out by Anggara *et al* (2015) have tried to combine DSM data from SRTM with DEM data to estimate the volume of stands, but there has been no broader research related to comparisons of different DSMs for the same purpose, as well as comparison with models based on optical spectral information such as vegetation index transformations.

The objectives of this study were twofold: (a) to develop a DSM-based vegetation volume index and to correlate it with the vegetation-sensitive transformations like NDVI, SAVI and FCD; (b) to evaluate the accuracy of DSM-based volume index as a basis for vegetation density parameter using forest cover density (FCD) as a reference.

2. Methods

This study departed from the assumption that the DSM represents the surface height of land cover including vegetation. Because the information provided is in the form of land cover surface height, there is a height difference between the DSM and the DEM, where the altitude value on the DSM should be higher. By calculating the difference between the DSM and DEM values, the value of the land cover surface height can be obtained. Multiplication of the height difference and the surface area generates land cover volume. Given that land cover in the form of vegetation differs from building land cover, since it is not massive and the underside is not completely covered with leaves, this volume value should be viewed as a volume index, that is, an index that represents volume, but not the volume value itself. The volume index was then compared with SAVI dan NDVI and correlated with the vegetation cover density represented by the FCD as a basis for regression model.

Study Area and Materials

The Menoreh Mountains area covering the districts of Kulon Progo and Purworejo was chosen as the research area based on the consideration that this area might represent an area with very rough topographic variations, so it is suitable to be a test of the reliability of DSM, DEM and vegetation spectral transformations in presenting information related to vegetation density. The image of the area is presented in the form of a false-color composite image of Landsat 8 OLI in Figure 1.

We used three types of digital surface model (DSM) images obtained using optical and radar spectra recording, namely ASTER GDEM optical image (30 m), Shuttle Radar Topography Mission (SRTM, 30 m), and ALOS PALSAR (30 m). In addition to the three types of DSM images, this study also utilized Landsat series imagery with a spatial resolution of 30 m, which were recorded in three different years, *i.e*., Landsat 7 ETM+ of 21 August 2002, Landsat 5 TM of 19 October 2009, and Landsat 8 OLI of 22 February 2015. This study selected these three image datasets with respect to the nearly cloud free coverage and the closest years to each DSM development, *i.e.,* SRTM (2000), ASTER GDEM (2009) and ALOS PALSAR (2014) respectively. As a reference DEM, we used RBI topographic map of 1:25,000 scale. The study area covers mountainous, hilly, and flat areas, which are covered by natural and semi-natural vegetation, as well as agricultural crops and settlements. All image processing stages were carried out using Idrisi TerrSet and ILWIS, while the map presentation was carried out using ILWIS and ArcGIS.

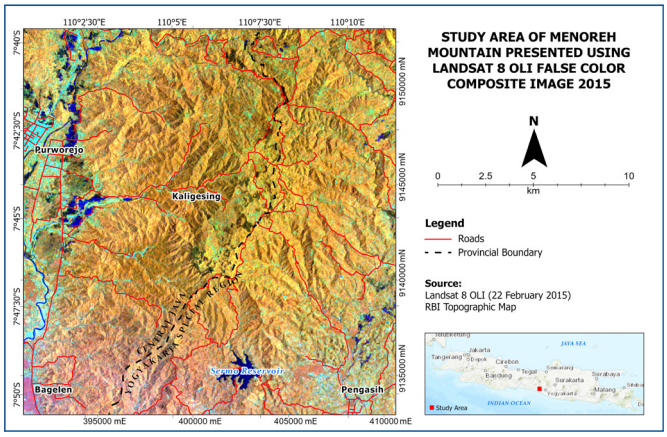

Figure 1. Study area as recorded by Landsat 8 OLI, using color composite of bands 5, 6, and 2 (RGB)

Research Stages

DEM Preparation

As summarized in Figure 2, in the initial stage the RBI topographic map was interpolated linearly to derive a digital elevation model (DEM) data. This DEM represents the spatial distribution of land surface elevations and becomes a reference for calculating the height difference (CHM or Canopy Height Model) and vegetation volume index (Volindex) based on the three DSM datasets. The pixel size of this reference DEM is set to 30 m in order to match the DSM datasets in this study.

Volume Index Development

In the second stage, each DSM was then overlaid with the reference DEM based on an assumption that the altitude on the land cover surface recorded in the DSM is equal to, or higher than, the elevation data available in the DEM image. Prior to doing this, each DSM image was converted to the projection system and its coordinates and datum, referring to the system used by the Indonesian Geospatial Information Agency (BIG). The result of subtracting the reference DEM pixel values from the DSM at the same position gives the height values of land cover in meters. By considering the area of each pixel, *i.e.,* 30 x 30 m^2, the product of the land surface area and the land-cover height gave the value of the volume of land-cover per pixel. Given that the volume values range very widely, a natural logarithmic function applied as follows:

$$Volindex = \ln((DSM - DEM) * Rs^2) \quad (1)$$

where Volindex is the volume index of the land cover volume, DSM is the land cover height in meter, DEM represents the ground elevation, and Rs is the spatial resolution in meter.

Vegetation Index Transformation

In the third stage, volume index images based on ASTER, SRTM, and ALOS Palsar were then compared with vegetation indices of NDVI and SAVI, as well as with FCD model based on the spectral transformation of Landsat series images. These indices have been known to have strong correlation with biomass content, stand volume, and carbon storage (Margaretha *et al*., 2013; Dewa and Danoedoro, 2017; Pahlevi *et al*., 2021; Zheng *et al.,* 2022). Prior to the application of

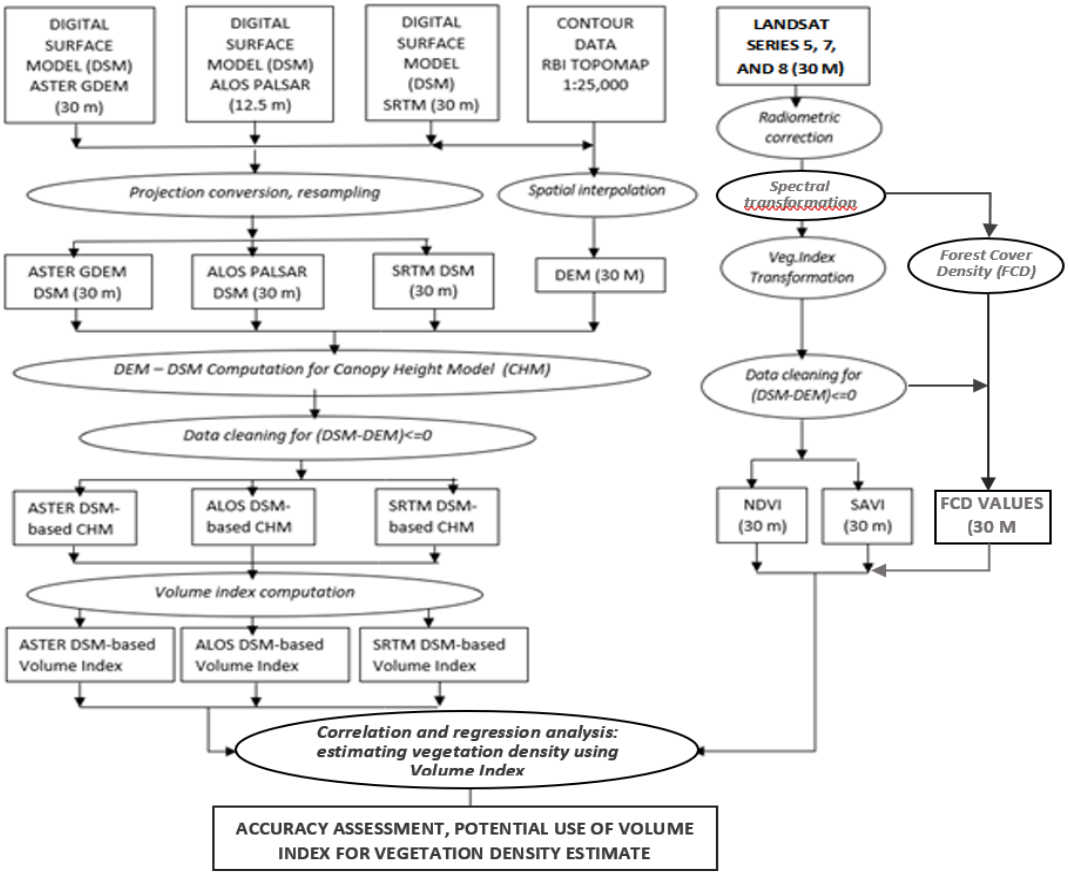

Figure 2. Flowchart of research methods

vegetation index and FCD transformations, all Landsat datasets were radiometrically corrected using 'full model' referring to Chavez (1996) and Eastman (2020), where the pixel values are transformed to at-surface reflectance ρ:

$$\rho = \frac{(\Pi * (L_\lambda - L_{haze}))}{(\tau_v * (E_o * Cos(T_Z) * \tau_z + E_{down})} \quad (2)$$

where ρ is at-surface reflectance in percent, L_λ is the image spectral radiance, L_{haze} is scattered spectral radiance recorded as the minimum one by the sensor, τ_v is the atmospheric transmittance or optical thickness of the atmosphere, E_o is the solar spectral irradiance which takes into account the Earth-Sun distance in specific Julian day, T_z is the incident angle of the direct solar flux to the Earth surface, and E_{down} is downwelling spectral irradiance due to the scattered solar flux in the atmosphere.

Practically, this correction takes into account image metadata containing information about (a) the range of the original DN values or the level of bit-coding, (b) maximum and minimum spectral radiance in Watts $m^{-2}sr^{-1}\mu m^{-1}$ that can be detected by the sensor, (d) Sun elevation and azimuth, (e) recording time (date, month and hour) follows the UTC standard, (f) optical thickness of the atmosphere at the time of recording, and (g) DNs for objects in the form of very dark shadows or very clear and deep water.

Meanwhile, the formulas for NDVI and SAVI are as follows:

$$NDVI = \frac{(Near\ Infrared - Red)}{(Near\ Infrared + Red)} \quad (3)$$

$$SAVI = \frac{Narr\ Infrared - Red}{Near\ Infared + Red + L} \times (1 + L) \quad (4)$$

where for both types of indices, the value ≤ 0 indicates non-vegetation land cover, 0 indicates barren land, while the greater the index value close to +1 indicates the higher vegetation density. The results of the correlation analysis then became the basis for evaluating the possibility of the DSM-based volume index to be used for estimating vegetation parameters.

Vegetation Density Reference Model using Forest Cover Density (FCD)

In this study, a field reference to represent vegetation density made use of Forest Cover Density (FCD) concept, although we ran it using ILWIS and Idrisi TerrSet instead of the FCD Mapper software. The FCD transformation (Rikimaru *et al*., 2002) makes use of six Landsat spectral bands, comprising blue, green, red, near infrared (NIR), first middle infrared (SWIR1) and thermal regions. The FCD model was developed using several stages of transformation, involving Advanced Vegetation Index (AVI), Soil Brightness Index (BI), Shadow Index (SI) and Thermal Index (TI). Combination of AVI and BI produces Vegetation Density (VD), while integration SI and TI generates Shadow Scaled Index (SSI). The FCD was computed using inputs from VD and SSI. The FCD is not simply an index like NDVI or SAVI, since it represents two aspects of vegetation parameters, *i.e.,* density and structural composition, so that it is frequently used for regional mapping of forest vegetation cover without correlating the values with the field measurement (ITTO, 1997). The following formulas follow an explanation from Rikimaru *et al*. (2002), Himayah *et al.* (2016) and Danoedoro and Gupita (2022).

AVI makes use of red and NIR bands and is formulated as follows.

IF (NIR-Red) ≤ 0,
THEN AVI= 0,
ELSE

$$AVI = \sqrt[3]{(NIR + 1) * (256 - Red) * (NIR - Red)} \quad (5)$$

BI makes use of blue, red and SWIR1 bands, and is formulated as follows:

$$BI = \left(\left(\frac{(SWIR1+Red)-(NIR+Blue)}{WIR1+Red)+(NIR+Blue)} \right) * 100 \right) + 100, \text{ Where } 0 \le BI \le 200 \quad (6)$$

SI image was generated by involving blue, green, and red bands, with the following formula:

$$SI = \sqrt[3]{(256 - Blue) * (256 - Green) * (256 - Red)} \quad (7)$$

While TI was derived from the rescaled thermal band.

We processed VD by applying a principal component analysis (PCA) of a dataset containing AVI and BI images. The VD was taken from the first principal component (PC1). The same approach applied for deriving SSI, where the first PC of SI – TI combination was taken. The VD was then rescaled to 0 – 100, where 0 represents bare soil (no vegetation) and 100 represent very dense vegetation. Areas with SSI value = 0 were regions with shadow value (SI) = 0 too. The area where SSI = 100 was the area with 100% shadow cover. The resultant FCD may have 0-100 range, depending on the vegetation density variation in the image, and was generated using the following formula

$$FCD = \sqrt{(VD \times SSI + 1)} - 1 \quad (8)$$

After that, the resultant FCD image was converted into classified FCD shown in Table 1.

3. Results and Discussion

DEM preparation through RBI contour interpolation

The DEM map resulting from the interpolation of RBI contour lines showed a variation of the ground surface elevation. Referring to the principle that 1: 25,000 scale contour maps can be rasterized with the smoothest spatial resolution of 1/2000 x the scale denominator (Tobler, 1988; McCloy, 2005), the allowable pixel size is 12.5 m or coarser. By using 30 m pixel size for the results of rasterization and interpolation of the formation of this DEM, the existing principles were not violated. The DEM map is presented in Figure 3, together with the DSM images of ALOS Palsar, ASTER GDEM, and SRTM respectively.

As shown in Figure 3, the maximum elevation of the reference DEM is 849 m, while the maximum values vary in the three DSMs. ALOS Palsar and SRTM maximum elevations are higher than the reference DEM, *i.e.,* 863 m and 657 m respectively, while the one of ASTER GDEM is lower than the reference, *i.e.*, 843 m. At a first glance, this elevation ranges give the impression that ASTER GDEM provides less accurate information, given that the DSM was built based on optical (near infrared) bands taken stereoscopically, which has no vegetation canopy penetration capability. On the contrary, the ALOS PALSAR and SRTM DSMs precisely perform higher maximum elevation values. Apart from these differences, correlation analysis between datasets showed that they are perfectly correlated with r = 1.0, which means that every increase in any location of one image is followed by increases in corresponding location of other images.

Volume Indices based on DSM Images

Canopy Height Model (CHM) was generated by subtracting the reference DEM from each DSM image. As shown in Figure 3. Many pixels in each CHM image have negative values, which is impossible to represent the canopy height or even any other land-cover, so that they are assigned a blank value. There are three possible errors related to this. First, the RBI topographic map which was used as a reference DEM is not accurate; second, all the satellite-based DSM images are not accurate; and the third is both types of datasets are not accurate.

Figure 3 shows that all CHMs have significant number of pixels containing negative values, although the height ranges are different, where SRTM represents the largest range. On the other hand, the highest average height difference belongs to ASTER GDEM, *i.e*, at 7.13 m. This phenomenon is probably related to the way ASTER GDEM acquired (using optical NIR spectrum), while the other two used radar wavelength, regarding that Almeida-Feilho *et al*., (2009), Kenyi *et al.,* (2009), Basuki *et al*., (2013), and Urbazaev *et a*l. (2018) mentioned that the microwave energy can penetrate the vegetation canopy. It

Table 1. FCD Classification according to ITTO, which contains density and structural composition

Class	Value Range	Vegetation structural composition description	Cls	Value Range	Vegetation structural composition description
0	0	Bare soil			
1	1-10	No canopy coverage. Open land and grass are predominant	6	51-60	Adult and young tree canopies are growing, covering 51-60% of the pixel area which is starting to show a difference
2	11-20	Tree canopies began to appear, but open land is still predominant	7	61-70	Tree canopies are growing rapidly covering 61-70% of the pixel area with differences in strata of stands, clearly visible and heterogeneous
3	21-30	Tree canopies occupy 11-20% of the pixel area but open land is still predominant	8	71-80	Tree canopies cover 71-80% of the pixel area with distinct strata standing distinctions, species heterogeneity is increasing,
4	31-40	Tree canopies occupy 21-30% of the pixel area interleaved with bushes and shrubs	9	81-90	Tree canopies cover 81-90% of the pixel area with different standing strata; very clearly seen, very high heterogeneity
5	41-50	Young tree canopies develop and cover 41-50% of the pixel area, with a predominance of shrubs while shrubs decrease.	10	91-100	Tree canopies cover 91-100% of the pixel area with very stratified differences, very high heterogeneity, sunlight is unable to reach the forest floor and moisture is very high.

Source: ITTO (1997)

is also interesting to note that the three CHMs depict different spatial pattern of pixels with positive values. The ALOS-based CHM show relatively random pattern of positive values and only occupies 11.12% of the total area. On the other hand, the ASTER GDEM-based and SRTM-based CHMs represent negative values in many parts of east- and southeast-facing slopes, although the ASTER's have more positive values in the flat and gently sloping areas. The negative values of the ASTER's occupies 61.66%, while the SRTM's covers 77.11% of the total area. To say it in another way, the three CHM models can only work in relatively small portion of the study area, when they are processed further for vegetation density analysis.

The CHM images were then trasformed to Volindex images by using equation (1). The result is presented in Figure 4. As compared to the correlations between CHMs, the correlation coefficients between VolIndices are lower. Figure 4 also shows that Volindex of ASTER GDEM is higher than others across the study area. It is not easy to find the reason why, because there is no information on the exact date of the data acquisition of the ASTER images that has been used for building up the GDEM, especially in relation with the presence of annual crops (planting period) and forest stands (*e.g.* seasonal deciduous). The same reason also applied for the other DSM images. A correlation matrix was developed for three Volindex images contaianing positive height values only. In contrast to the original DSM images, the correlation coefficients between Volindex images become much lower, which means that their variation in space and time are different. Generally speaking, the SRTM-based Volindex model has the highest value range as compared to that of ALOS-Palsar and ASTER GDEM.

Vegetation Indices Development

Two vegetation indices, *i.e.* NDVI and SAVI were generated using three different datasets of Landsat. Radiometric correction were applied to the datasets that has not been correctited using equation (2), and the NDVI and SAVI images were derived using equaitons (3) and (4). For image with the closest date of recording to SRTM data development (and relatively cloud free), a Landsat 7 ETM+ of 2002 has been used, while for ASTER GDEM a Landsat 5 TM of 2009 dataset was chosen, and for ALOS PALSAR a Landsat 8 OLI of 2015 was selected. They do not exactly match the years or dates of DSM development, but they are recorded at the closest dates of recording with relatively good quality, although the thermal bands of Landsat 7 ETM+ and Landsat 5 TM are not good enough. The resultant images are presented in Figure 4.

Vegetation Cover Density

Vegetation cover density as a reference for the DSM-based volume index modelling was built up using forest cover

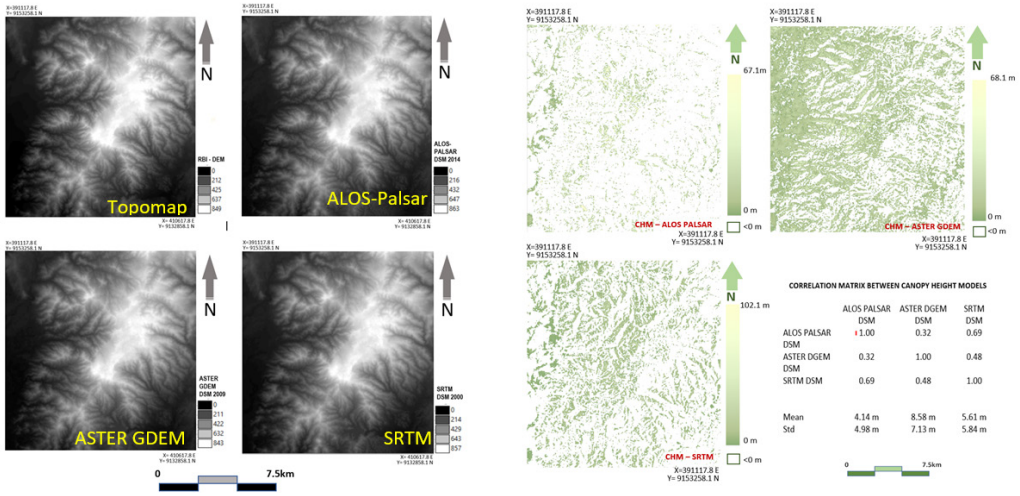

Figure 3. Left: The (DEM) and DSM. Right: Comparison betwen Canopy Height Models (CHMs) generated using three DSMs

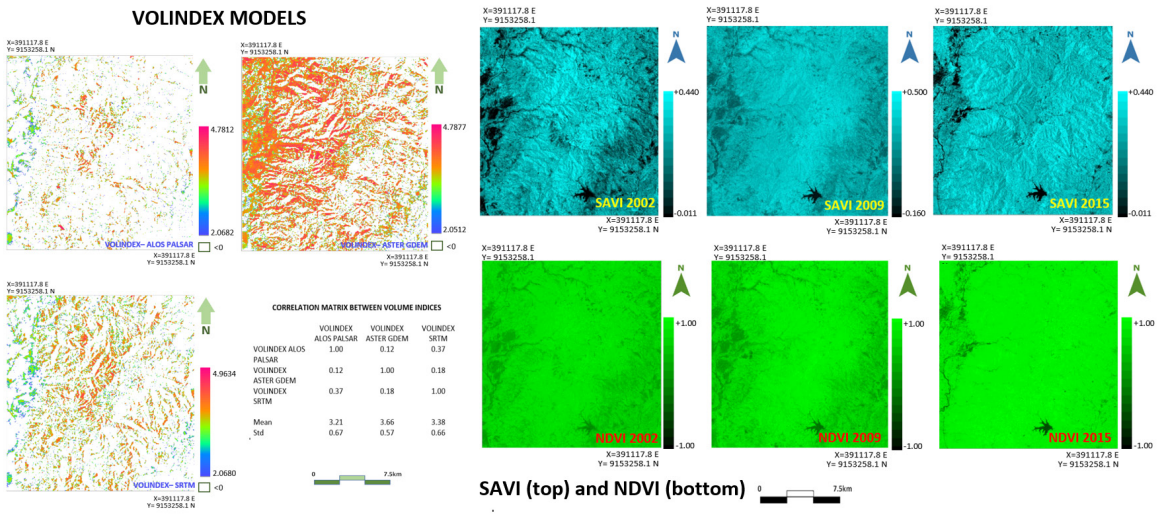

Figure 4. Left: Comparisan between Volindix images generated using ALOS Palsar, ASTER GDEM, and SRTM. Right: SAVI and NDVI images of different years corersponding with the year of DSMs acquisition.

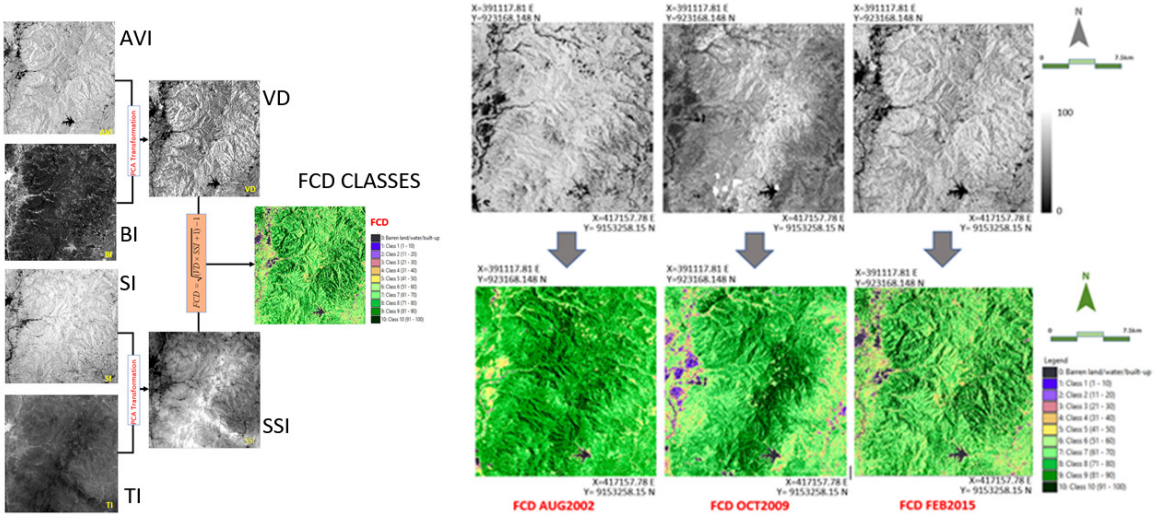

Figure 5. Left: Example of vegetation cover density model developed using several stages involving six indices 2015. Right: Three FCD images in real values (top) and classified maps used as field references

density (FCD) transformation. Figure 5 depicts the outline of the process carried out in this study, where the vegetation cover density is represented by FCD and was generated using Advanced Vegetation Index (AVI), Bare Soil Index (BI), Shadow Index (SI), Thermal Index (TI), Vegetation Density (VD), and Shadow-scaled Index (SSI). This procedure applied for three dates of recording with respect to the use of three different DSMs. The formula for these indices refer to equations (5) up to (8). All FCD formulas work on the 8-bit Landsat data, so that all images were rescaled to 0-255 range first (Danoedoro and Gupita, 2022). The Vegetation Density (VD) index was generated using principal component analysis (PCA) involving dataset containing AVI dan BI, while the Shadow-scaled Index (SSI) was derived using PCA of dataset containing SI and TI. The process of VD and SSI generation using PCA required inversions since the results showed inversed pixel values, i.e. the original PC1 of VD and SSI performed high values for bare soil and low ones for vegetation. Therefore, we applied inversion followed by 0-100 rescaling.

Referring to ITTO (1997) and Rikimaru *et al (*2002), the FCD model is a semi-expert sytem, which was developed for forest cover density mapping with limited or the absent of field survey, since the formulas involved were based on empirical information and purposively designed for covering remote areas. Therefore, this study made use of the FCD models of 2002, 2009, and 2015 as references for the DSM-based Volindex models being evaluated. However, this study also found that three FCD models are not exactly the same in representing the condition of vegetation cover, both in density and structural composition. Figure 5 represents the three FCD maps.

Figure 5 also shows that there are some differences among the vegetation density of 2002, 2009 and 2015 which are represenetd by the FCDs. The FCD map of 2002 looks less contrats as compared to the other years. Besides, the FCD map of 2009 shows denser vegetation classes on the east-facing slopes. The FCD map of 2015 represents sparser vegetation density and accentuates the relief expression of the study area. These differences were caused, for one thing, by the difference in time recording as well as the level of atmospheric disturbance. In addtion, the seasons of recording also imply the greeness level of the vegetation. For example, in 2002 the vegetation cover of the study area was relatively better than the more recent condition. On the other hand, October is the end of dry season, and most annual crops and dediduous vegetation are usually have low greeness levels. The quality of Landsat 7 ETM+'s thermal band also affected the derivation of the FCD of 2002, particularly in building up the TI and SSI, so that the urban areas look more vegetated than those of 2009 and 2015.

Since the FCD concept combines percentage of vegetation coverage and the structural composition, it was not easy to validate the exact values of the model (at 0–100 range) using vegetation density measurement in the field. That is why the authors could only validate the FCD classes wih the field observation, which took into account the density and the structural composition at once. Problem occured when there was no accurate information on the vegetation density and structural compositon during the years of recording. Interview with the local people supported by the assumption that in mountainous and remote areas the forest cover did not change significantly applied in this situation. By using confusion matrix, we found that the accuracy levels of the FCD model are 76.34% for 2002, 85.01% for 2009, and 84.74% for 2015, which are similar to result obtained by Danoedoro and Gupita (2022). Regardless this accuracy level, we used these information as a basis for correlation with the Volindex models.

Correlation and Regression Analysis between Vegetation Density and Volindex Models

After obtaining all DSM-based Volindex and vegetation density models, the authors applied masking for all maps in order to exclude areas with negative values with regard to the Volindex models of SRTM, ASTER GDEM, and ALOS Palsar. That is to say, only relatively few pixels were involved in this analysis since the Volindex negative values implied the impossibility to model the vegetation density. Table 2 represent the correlation matrix between all vegetation indices (NDVI and SAVI), FCD, and Volindex of all years involved. Therefore, this correlation analysis at this stage was based on the population involving millions of pixels, instead of samples.

As shown in Table 2, correlation between NDVIs varies with the years of recording. The lowest correlation coefficient was presented by NDVI 2002 and NDVI 2015, while the highest one was between NDVI 2002 and NDVI 2009. The same pattern was also presented by SAVIs, which means that the vegetation density (regardless the structural composition) of the study area changed significantly over time of observation. When the

vegetation structural composition was also involved, we found that the highest correlation coefficient between FCDs belongs to the same pair as NDVI's and SAVIS's (*i.e*. FCD 2002 and FCD 2009, at 0.62). To say it in another way, the vegetation density of the study area performed the same pattern as viewed from cover percentage as well as from structural composition.

When the Volindex models were correlated with the vegetation indices and FCD models, slight differences in correlation were found, although the Volindex ALOS performed the best and the Volindex ASTER was the worst. The NDVIs have low correlation coefficient with all Volindex models. The highest coefficient was performed by the Volindex ALOS and NDVI 2015. SAVIs gave stronger correlations with Volindex of ALOS, as compared to other Volindex models, In terms of vegetation density represented by the FCDs, the Volindex of ALOS performed a relatively higher correlation coefficient with all FCD models, despite the FCD 2002 - Volindex ALOS pair shows weak correlation (at 0.43) and the FCD 2009 – Volindex ALOS as well as FCD 2015 – Volindex ALOS pairs perform moderate correlation at 0.50 and 0.51 respectively. The SAVI 2015 strongly correlates with the FCD 2015 at r=0.97, and consistently the SAVI 2015 correlates with the Volindex ALOS. Since this study focused on the vegetation density parameter representing a combination between cover density and structural composition, we used correlation between Volindex ALOS and all FCD models for further analysis.

At the next stage, we took samples from the FCD models to represent the vegetation density parameters in the field and we extract the Volindex values at the corresponding locations. For each pair of FCD – Volindex we selected different sample sets, due to the fact that the pixels representing DSM with posirive values are distributed differently among sensors. Therefore there were 30 sample points for each Volindex model 3.

Since the Volindex ASTER performed the worst correlation coefficients with all FCD models, this study made use the pairs of Volindex SRTM – FCD 2002, Volindex ALOS – FCD 2009, and Volindex ALOS – FCD 2015 to represent the best correlations as the basis for vegetation density estimate using regression equations. Prior to the corelation and regression analyses, a normality test applied, and we found the samples could be used for the regression analysis. In contrast to the total population involved in the correlation matrix (Table 2), the analyzed samples showed a relatively higher correlation for each pair of Volindex and FCD. The authors found that the Volindex SRTM – FCD 2002 has a positive correlation with r =0.489, which is very close to the moderate level. Meanwhile, the Volindex ALOS – FCD 2009 and Volindex – FCD2015 have positive correlation at r = 0.565 and r = 0.640 respectively. Although these correlation coefficients are not high enough, we still need to test the regression equation for predicting the vegetation density values using Volindex of SRTM and ALOS. The results are presented in Table 3.

The regression equations for modelling the vegetation densit parameter in terms of FCD were obtained using Volindex SRTM (for Landsat 7 ETM+ of 2002) and Volindex ALOS (for Landsat 5 TM of 2009 and Landsat 8 OLI of 2015). Table 3 also shows the selected equations in the rightmost column. After that, these regression equations were run separately using map calculator for generating predicted or estimated FCDs. The results are presented in Figure 6, where the spatial distribution of each estimated FCD shows different pattern and values, depending on the positive values obtained from the CHM previously explained.

Accuracy Assessment of the Results

Acuracy assessment of the estimated or predicted FCDs applied two methods to the different products. Firstly, the predicted FCD values were assessed using standard error of estimate (SEE). Based on the SEE, the minimum and maximum accuracies were calculated according to the 95% confidence level. Secondly, the pedicted FCD classes were evaluated using confusion matrix (Congalton and Green, 2009), and gave results in overall accuracy as well and Kappa. Both methods made use of independent datasets, taken from the originally generated FCD maps explained in section 3.5.

As presented in Table 3, the SEE of the 2002 result using SRTM-based Volindex is 47.26, while the SEEs of 2009 and 2015 results using ALOS-based Volindex are 36,11 and 29.78 respectively. These SEEs gave maximum accuracys at 24.55%, 34,25% and 39.44%; and 27.24%, 37.22% and 44.75% respectively. In terms of the FCD classes, the overall accuracies obtained are 30.04% (for SRTM-based Volindex), 37.27% and 41.54% (for ALOS-based Volindex). .

The accuracy assessment implies that all Volindex model cannot accurately predict the vegetation density parameter, which is represented by the FCD models. The most accurate Volindex model, *i.e*. the ALOS Palsar-based Volindex could only reach 41.53% overall accuracy when it is transformed into

Table 2. Correlation matrix between all vegetation indices, FCD and Volindex models

		NDVI			SAVI			FCD			VOLINDEX		
		2002	2009	2015	2002	2009	2015	2002	2009	2015	SRTM	ASTER	ALOS
NDVI	2002	1.00	0.87	0.48	0.83	075	0.31	0.69	0.72	0.30	0.21	-0.04	0.24
	2009	0.87	1.00	0.55	0.72	0.82	0.33	0.58	0.79	0.32	0.24	-0.03	0.28
	2015	0.48	0.55	1.00	0.47	0.52	0.77	0.41	0.46	0.71	0.22	0.00	0.23
SAVI	2002	0.83	0.72	0.47	1.00	0.77	0.46	0.82	0.79	0.46	0.31	0.13	0.42
	2009	0.75	0.82	0.52	0.77	1.00	0.43	0.60	0.87	0.41	0.23	0.10	0.54
	2015	0.31	0.33	0.77	0.42	0.43	1.00	0.42	0.46	0.97	0.26	0.12	0.52
FCD	2002	0.69	0.58	0.41	0.82	0.60	0.42	1.00	0.62	0.42	0.35	0.12	0.43
	2009	0.72	0.79	0.46	0.79	0.87	0.46	0.62	1.00	0.47	0.27	0.09	0.51
	2015	0.30	0.32	0.71	0.46	0.41	0.97	0.42	0.47	1.00	0.32	0.03	0.52
VOL-INDX	SRTM	0.29	0.24	0.22	0.32	0.23	0.26	0.35	0.27	0.32	1.00	0.17	0.37
	ASTER	-0.04	0.14	0.00	0.13	0.10	0.12	0.09	0.31	0.08	0.17	1.00	0.12
	ALOS	0.24	0.28	0.31	0.42	0.44	0.52	0.43	0.50	0.51	0.37	0.12	1.00

Note: SRTM was acquired in 2002, ASTER GDEM in 2009, and ALOS Palsar in 2014

Table3.SamplesofFCD–Volindexpairs

Smpl No	FCD2002-SRTM		FCD2009-ALOS		FCD2015-ALOS		Correlation coefficients and regression equation
	FCD2002	VOLIDX SRTM	FCD2015	VOLIDX ALOS	FCD2009	VOLIDX ALOS	
1	11.50	2.073	0.000	2.042	10.30	2.042	For SRTM-based DSM and L7 ETM+:
2	78.90	4.441	44.440	2.998	52.51	2.998	
3	99.40	4.912	89.940	4.681	77.66	4.681	FCD = 269.1 + 0.016*Volindex_SRTM
4	0.00	2.451	75.730	4.392	89.92	4.392	
5	44.60	2.002	40.060	3.247	47.23	3.247	R^2 = 0.239
6	34.70	3.744	8.920	4.555	90.12	4.555	
7	22.80	3.949	10.550	3.007	84.83	3.007	
8	85.10	4.953	36.720	2.568	56.32	2.568	
9	69.80	2.006	69.690	4.282	43.45	4.282	
10	87.50	3.252	88.920	4.556	65.21	4.556	
11	54.60	2.989	92.930	3.966	24.29	3.966	For ALOS-based DSM and L5 TM:
12	17.90	3.225	76.110	4.112	27.88	4.112	
13	75.70	3.995	89.950	4.004	88.32	4.004	FCD = -3.255 + 15.067*Volindex_SRTM
14	29.30	3.012	14.350	2.045	12.24	2.045	
15	40.60	4.747	50.010	2.234	50.31	2.234	R^2 = 0.319
16	4.90	2.003	46.160	3.201	35.32	3.201	
17	90.90	3.955	67.390	2.006	45.18	2.006	
18	79.40	3.245	42.620	2.567	66.55	2.567	
19	63.80	4.965	28.280	2.223	35.75	2.223	
20	61.60	3.002	59.330	3.457	65.63	3.457	
21	33.30	3.248	26.340	2.038	64.08	2.038	For ALOS-based DSM and L8 OLI:
22	0.00	2.342	0.230	2.345	39.27	2.345	
23	10.70	3.007	2.740	2.331	26.36	2.331	
24	81.80	2.989	3.480	3.452	70.01	3.452	FCD = -0.470 + 15.466*Volindex_ALOS
25	49.50	3.647	12.830	2.221	24.11	2.221	
26	60.60	4.879	39.750	2.573	0.98	2.573	R^2 = 0.410
27	35.50	4.646	20.780	2.023	11.89	2.023	
28	4.94	2.505	62.350	3.695	42.67	3.695	
29	41.25	4.365	24.280	2.705	29.39	2.705	
30	20.47	3.754	33.280	2.676	34.13	2.676	

Note The Volindex of ASTER GDEM was not used due to its very low correlation with all FCDs, and replaced by Volindex of ALOS which shows relatively higher correlation with FCD 2009 and FCD 2015

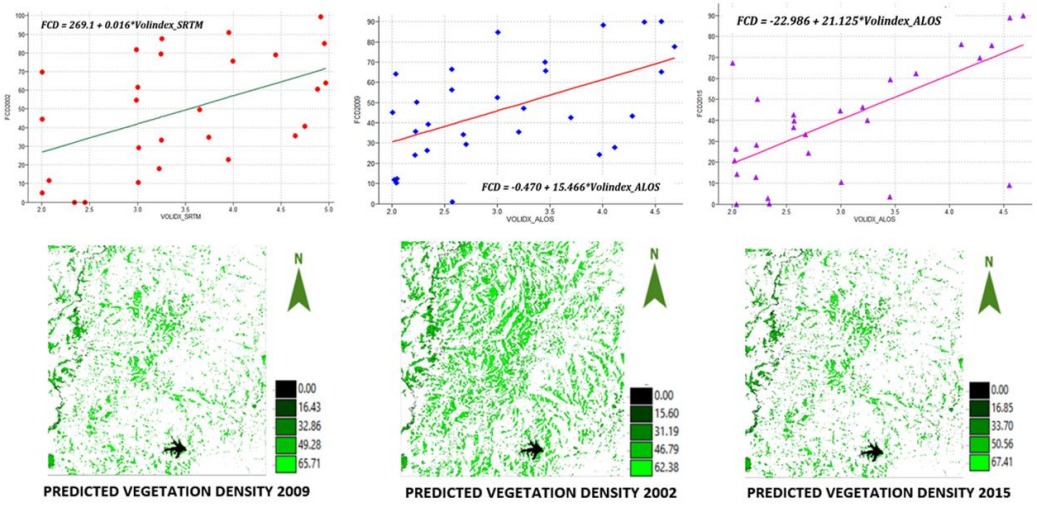

Figure 6. Regression equations used for transforming the Volindex models into prediceted FCDs.

FCD classes. Apart from this weakness, the ALOS Palsar-based Volindex model could be used to predict the vegetation density parameter of different years at relatively higher accuracy as compared to the other Volindex models. Among the three models, the ASTER GDEM-based one was found the worst since it shows very low correlation coefficient with the vegetation indices and FCD. Figure 7 depicts the most accurate model.

The low accuracy of the Volindex model might be caused by several factors, *i.e*. the accuracies of RBI topographic map, the satellite-based DSMs, and the FCDs. In addition, Landsat images

Table 4. Standard Error of Estimates and accuracies of the predicted FCD based on Volindex models

Volindex and Predicted FCD	SEE	Minimum accuracy	Maximum accuracy	Overall accuracy	Kappa
FCD 2002 (based on Volindex SRTM)	47.26	22.25%	24.24%	29.04%	0.2853
FCD 2009 (based on Volindex ALOS)	35.11	34.55%	37.22%	37.27%	0.2498
FCD 2015 (based on Volindex ALOS)	29.78	39.44%	44.74%	41.53%	0.3902

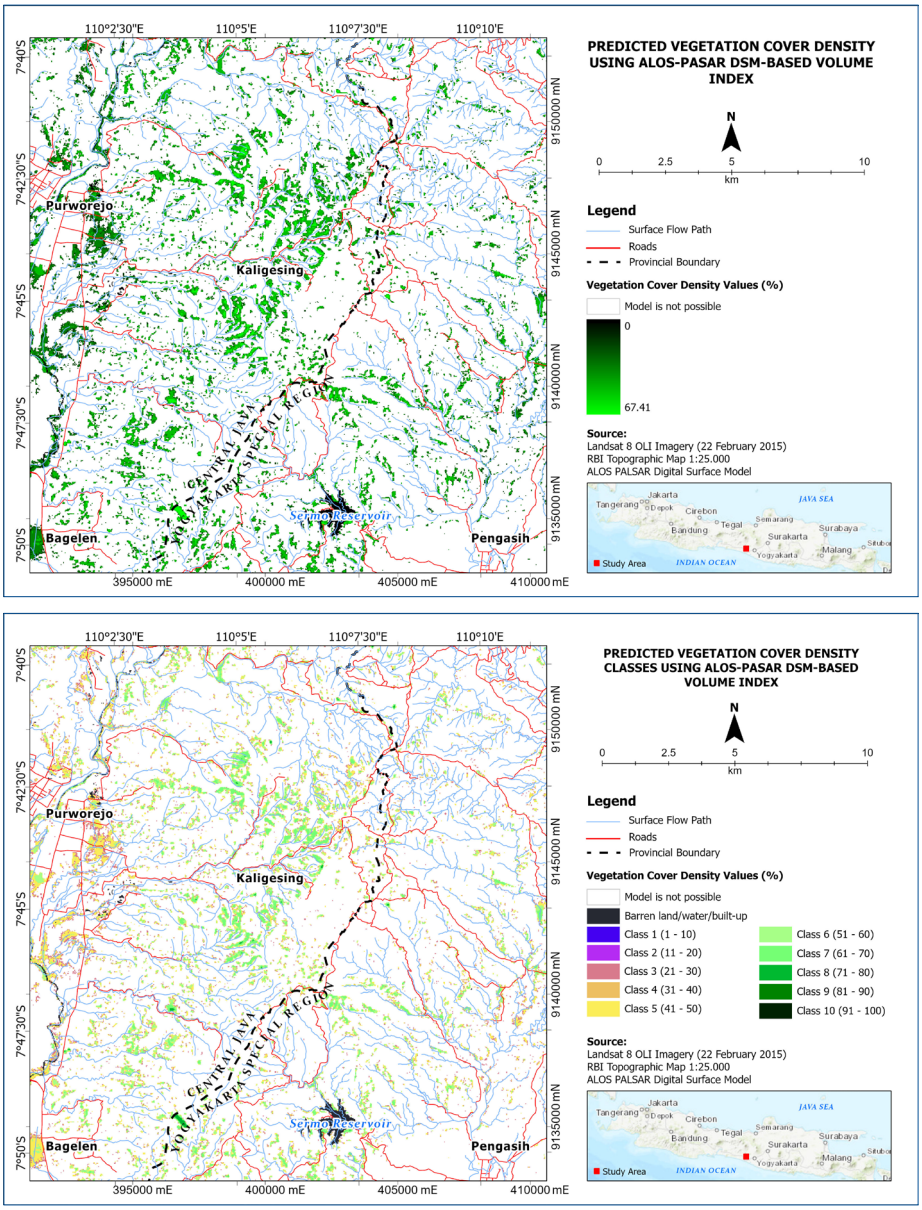

Figure 7. Predicted vegetation cover density using Volindex of ALOS Palsar. Top: real values, bottom: classified values to structural composition categories (see Table 1)

quality and the topographic configuration of the study area might play an important role. With 12.5 m contour intervals, the maximum acuracy of the RBI topographic map and the derive DEM is only 6.25 m (Robinson *et al.,* 1995; Hugget and Cheesman, 2002). The resultant CHMs show that many pixels with negative values exist, indicating that most of the SRTM, ASTER GDEM, and ALOS Palsar's elevation values are lower than the RBI topographic map's ground elevation. Different patterns of the CHMs' negative values also indicate a systematic inaccuracies, which require further studies. Different Landsat datasets also perform different ranges of NDVI and SAVI, which means that they need relative calibrations. Extremely rough topography of Menoreh Mountain also caused radiometric bias, which has been studied by Umarhadi and Danoedoro (2019; 2020). This bias might lead to inaccuracies of the derived FCD models.

4. Conclusions

This study found that the Volindex concept does not work well as a basis for vegetation density estimation or prediction in very rough topography like Menoreh Mountain. The negative values that are performed by the CHMs cause Volindex models can only work in several topographic parts of the study area, depending on the satellite sensors used. Correlation analysis showed that the Volindex models more correlate with the FCDs than with NDVIs and SAVIs, although there is no strong correlation between them. As compared to other DSMs, the ALOS Palsar DSM could generate Volindex models that are more

correlated to all FCDs of all years, and the best correlation can be used for predicting the vegetation cover density at 41.54% overall accuracy. There is a need for further studies in other areas with various topographic characteristics and using more accurate topographic map as basis for CHM and Volindex computation. In addition, radiometric calibration in terms of topographic correction of the multispectral data should also be considered.

Acknowledgement

This study was supported by the Independent Research Program of the Faculty of Geography, Universitas Gadjah Mada. The authors would like to thank the anonymous reviewers for their criticism and valuable suggestions.

References

R. Almeida-Filho, R., Shimabukuro, Y.E., Rosenqvist, A., and Sánchez, G.A. (2009). Using dual-polarized ALOS PALSAR data for detecting new fronts of deforestation in the Brazilian Amazônia. Intrenational Journal of Remote Sensing, 30, (14): 3735-3743, DOI: 10.1080/01431160902777175

Anggara, D.W., Wicaksono, P., and Danoedoro, P. (2015). The Integration of Active and Passive Remote Sensing System: Mapping Forest Stand-Volume Using ALOS AVNIR-2 and SRTM Data. *Prosiding* Pertemuan Ilmiah Tahunan MAPIN XX, Bogor

Basuki, T.M. Andrew K. Skidmore, A. K., Hussin, Y. A., and van Duren, I. (2013). Estimating tropical forest biomass more accurately by integrating ALOS PALSAR and Landsat-7 ETM+ data. *International Journal of Remote Sensing,* 34, (13): 4871-4888, DOI: 10.1080/01431161.2013.777486

Chavez, P. S. (1996). Image-Based Atmospheric Corrections Revisited and Improved. *Photogrammetric. Engineering and Remote Sensing.*, vol. 62, no. 9, pp. 1025–1036, 1996,

Congalton, R.G. and Green, K. (2009) *Assessing the Accuracy of Remotely Sensed Data: Principles and Practices*. 2nd Edition, Lewis Publishers, Boca Raton.

Danoedoro, P. (2019). Multidimensional Land-use Information for Local Planning and Land Resources Assessment in Indonesia: Classification Scheme for Information Extraction from High-Spatial Resolution Imagery. *Indonesian Journal of Geography,* 51 (2): 131 – 146

Danoedoro, P., and Gupita, D.D. (2022). Combining Pan-Sharpening and Forest Cover Density Transformation Methods for Vegetation Mapping using Landsat-8 Satellite Imagery. *International Journal on Advanced Science, Engineering, and Information Technology*, 12, (3): 881-891

Dewa, R.P., and Danoedoro, P. (2017). The effect of image radiometric correction on the accuracy of vegetation canopy density estimate using several Landsat-8 OLI's vegetation indices: A case study of Wonosari area, Indonesia. *Proceedings* of the IOP Conference Series: Earth and Environmental Science (54): 1 012046

Drăguţ, L., Eisank, C., and Strasser, T. (2011). Local variance for multi-scale analysis in geomorphometry. *Geomorphology* (130): 162–172

Drăguţ, L., and Eisank, C. (2012). Automated object-based classification of topography from SRTM data. *Geomorphology* (142): 21–33

Eastman, J. R. (2020). Terrset 2020. *Geospatial Monitoring and Modelling System Manual*. Worchester, MA: Clark University

Hecht, R., Meinel, G., and Buchroithner, M.F. (2008). Estimation of Urban Green Volume Based on Single-Pulse LiDAR Data. *IEEE Transactions on Geoscience and Remote Sensing*, 46, (11): 1-11

Himayah, S., Hartono, Danoedoro, P.(2016). The Utilization of Landsat 8 Multitemporal Imagery and Forest Canopy Density (FCD) Model for Forest Reclamation Priority of Natural Disaster Areas at Kelud Mountain, East Java. *IOP Conference Series: Earth and Environmental Science*, 47(1), 012043

Huete, A.R. (1988). A Soil-Adjusted Vegetation Index (SAVI). *Remote Sensing of Environment* (25): 295-309

Huggett, R.G., and Cheesman, J. (2002). *Topography and the Enviroment*. Chichester: Prentice Hall.

Salsabila, H. N., and Danoedoro, P. (2021). Comparing Two Different Radiometric Corrections in a Vegetation Mapping of Mountainous Area using Forest Cover Density Transformation. Proceedings of the 42nd Asian Conference on Remote Sensing, ACRS 2021, Can Tho, Vietnam

Ismail, M., Hartono, and Danoedoro, P. (2017). "The Application of Forest Cover Density (FCD) Model for Structural Composition of Vegetation Changes in Part of Lore Lindu National Park, Central Sulawesi Province", In *Proceedings* of the 5th Geoinformation Science Symposium 2017. IOP Publishing IOP Conf. Series: Earth and Environmental Science (98) 012056

International Tropical Timber Organization (ITTO). (1997). Utilization of Remote Sensing in Site Assessment and Planning for Rehabilitation of Logged-Over Forests. *Project Report* on PD 32193 Rev.2 (F): Rehabilitation of Logged-Over Forests in Asia/Pacific Region, Sub-Project Iii.

Julzarika, J., and Harintaka (2019). Free Global Dem: Converting DSM to DTM and Its Applications. *The International Archives of the Photogrammetry, Remote Sensing and Spatial Information Sciences*, Volume XLII-4/W16, 2019 and 6th International Conference on Geomatics and Geospatial Technology (GGT 2019), 1–3 October 2019, Kuala Lumpur, Malaysia

Kellndofer, J. , Walkera, W., Pierca, L., Dobsona, C., Fitesb, J.A. (2008). Vegetation height estimation from Shuttle Radar Topography Mission and National Elevation Datasets. *Remote Sensing of Environment* (93): 339 – 358

Kenyi, L. Dubayah, R., Hofton, M., and Schardt, M. (2009). Comparative analysis of SRTM-NED vegetation canopy height to LIDAR-derived vegetation canopy metrics. *International Journal of Remote Sensing* 30,(11):2797-2811. DOI: 10.1080/01431160802555853

Margaretha, W., Danoedoro, P., Murti, S.H. (2013). Estimasi Cadangan Karbon Vegetasi Tegakan di Kota Yogyakarta dan Sekitarnya Berbasis ALOS AVNIR-2. *Prosiding Simposium Nasional Sains Geoinformasi* ~ III

McCloy, K.R. (2005). *Resource Management Information Systems: Remote Sensing, GIS, and Modelling.* 2nd edition. Broken Sound Parkway, NW: CRC Press

Nikolakopoulos, K. G., and Chrysoulakis, N. (2006). Updating the 1:50.000 topographic maps using ASTER and SRTM DEM. The case of Athens, Greece. *Remote Sensing for Environmental Monitoring, GIS Applications, and Geology VI*, *Proc. of SPIE* Vol. 6366, 636606, 0277-786X/06/$15 · doi: 10.1117/12.689016

Pahlefi, M.R., Danoedoro, P., and Kamal, M. (2021). The utilization of sentinel-2A images and google earth engine for monitoring tropical Savannah grassland. Geocarto International 39, (6): 1-15. https://doi.org/10.1080/10106049.2021.1914749

Prasannakumar, H. Vijith, S. Abinod, and N. Geetha. (2012). Estimation of soil erosion risk within a smallmountainous sub-watershed in Kerala, India, using Revised Universal Soil Loss Equation (RUSLE) andgeo-information technology. *Geoscience Frontiers* 3(2): 209-215

Rikimaru, A., Roy, P.S., & Miyatake, S. 2002. Tropical Forest Cover Density Mapping. *Tropical Ecology*. 43(1): 39-47.

Robinson, A. H., Morrison, J.L., Muehrcke, P.C., Kimerling, A.J., and Guptill, S.C. . (1995). *Elements of Cartography* (6th ed.). New York: John Wiley and Sons.

Taramelli, A., and Melelli, L. (2008). Detecting Alluvial Fans Using Quantitative Roughness Characterization and Fuzzy Logic Analysis. *CCSA 2008*, Part I, LNCS 5072: 1–15,

Trier, Ø. D. Salberg, A-B., Haarpaintner, J., Aarsten, D. (2018). Multi-sensor forest vegetation height mapping methods for Tanzania. *European Journal of Remote Sensing*, 51, (1): 587–606

Tobbler, W. (1988). Resolution, Resampling, and All That, In Mounsey, H., and. Tomlinson, R. (eds)., *Building Data Bases for Global Science*, London, Taylor and Francis.

Umarhadi, D.A., and Danoedoro, P. (2019). Correcting topographic effect on Landsat-8 images: An evaluation of using different DEMs in Indonesia. *Proceedings* of SPIE - The International Society for Optical Engineering, 11311, 113110L

Umarhadi, D.A., and Danoedoro, P. (2020). The effect of topographic correction on canopy density mapping using satellite imagery in mountainous area. *International Journal on Advanced Science, Engineering, and Information Technology*, (10), 3: 1317–1325

Umarhadi, D.A., Danoedoro, P., Wicaksono, P., Widayani, P., Nurbandi, W., Juniansah, A. (2018). The Comparison of Canopy Density Measurement Using UAV and Hemispherical Photography for Remote Sensing Based Mapping. *Proceedings* of the 4th International Conference on Science and Technology, ICST 2018, 8528670

Urbazaev, M., Cremer, F., Migliavacca, M., and Reichstein, M. (2018). Potential of Multi-Temporal ALOS-2 PALSAR-2 ScanSAR Data for Vegetation Height Estimation in Tropical Forests of Mexico. *Remote Sensing*, 10, 1277; doi:10.3390/rs10081277

Wu, M., Yang, C., Song, X., Hoffmann, W.C. (2004). Evaluation of Orthomosics and Digital Surface Models Derived from Aerial Imagery for Crop Type Mapping. *Remote Sensing of Environment* (93): 339 – 358

Zheng, W., Liu, Y. Yang, X., and Fan, W. (2022). Spatiotemporal Variations of Forest Vegetation Phenology and Its Response to Climate Change in Northeast China. Remote Sensing 14, (12): 2909. DOI: /10.3390/rs14122909